A genome-wide CRISPR/Cas9 knock-out screen identifies the DEAD box RNA helicase DDX42 as a broad antiviral inhibitor

Bonaventure Boris[1], Rebendenne Antoine[1*], Garcia de Gracia Francisco[1*], McKellar Joe[1*], Tauziet Marine[1], Chaves Valadão Ana Luiza[1], Courgnaud Valérie[2], Bernard Eric[1], Briant Laurence[1], Gros Nathalie[3], Djilli Wassila[1], Arnaud-Arnould Mary[1], Parrinello Hugues[4], Rialle Stéphanie[4], Moncorgé Olivier[1] and Goujon Caroline[1#]

1 IRIM, CNRS, Université de Montpellier, France

2 IGMM, CNRS, Université de Montpellier, France

3 CEMIPAI, CNRS, Université de Montpellier, France

4 Montpellier GenomiX (MGX), France

* contributed equally

[#] Corresponding and lead author: IRIM UMR9004, 1919 route de Mende, 34293 Montpellier cedex 5. Phone: +33 4 34 35 94 33, e-mail: caroline.goujon@irim.cnrs.fr, ORCID iD: 0000-0001-8571-1108

Abstract

Genome-wide CRISPR/Cas9 knock-out genetic screens are powerful approaches to unravel new regulators of viral infections. Here, we took advantage of the ability of interferon (IFN) to restrict HIV-1 infection, in order to create an environment hostile to replication and reveal new inhibitors through a CRISPR screen. This approach led to the identification of the RNA helicase DDX42 as an intrinsic inhibitor of HIV-1. Depletion of endogenous DDX42 increased HIV-1 DNA accumulation and infection in cell lines and primary cells, irrespectively of IFN treatment. DDX42 overexpression inhibited HIV-1, whereas a dominant-negative mutant of DDX42 increased infection. Importantly, DDX42 impacted retrotransposition of long interspersed elements-1 (LINE-1), infection with other retroviruses and positive-strand RNA viruses, including Chikungunya virus (CHIKV) and severe acute respiratory syndrome coronavirus 2 (SARS-CoV-2). However, DDX42 did not inhibit infection with negative-strand RNA viruses such as influenza A virus (IAV), arguing against a general, unspecific effect on target cells. Proximity ligation assays showed DDX42 in the vicinity of viral elements during infection, and RNA immunoprecipitation confirmed DDX42 interaction with LINE-1 RNAs. This strongly suggested a direct mode of action of DDX42 on viral ribonucleoprotein complexes. Taken together, our results identify DDX42 as a new, broadly active intrinsic antiviral inhibitor.

Introduction

Over the past 20 years, a growing list of cellular proteins with various functions have been identified as capable of limiting different steps of virus life cycles, including HIV-1 (Chemudupati et al., 2019; Doyle et al., 2015; Ghimire et al., 2018). Viruses have often evolved to counteract the action of these so-called restriction factors. However, type 1 interferons (IFNs) induce, through the expression of interferon-stimulated genes, an antiviral state particularly efficient at inhibiting HIV-1 when cells are pre-exposed to IFN (Doyle et al., 2015). The dynamin-like GTPase MX2, and, recently, the restriction factor TRIM5α, have both been shown to participate in this IFN-induced inhibition (Goujon et al., 2013a; Kane et al., 2013; OhAinle et al., 2018; Jimenez-Guardeño et al., 2019). With the hypothesis that additional HIV-1 inhibitors remained to be identified, we took advantage of the hostile environment induced by IFN to develop a whole-genome, CRISPR/Cas9 screen strategy in order to reveal such inhibitors. This strategy led us to identify DDX42 as a new intrinsic inhibitor of HIV-1, also capable of inhibiting a range of other positive RNA viruses.

Results

The Genome-Scale CRISPR Knock-Out (GeCKO) sgRNA library (Sanjana et al., 2014; Shalem et al., 2014, 2015) was used to generate knock-out populations in the glioblastoma T98G cell line. This cell line is both highly permissive to HIV-1 infection and potently able to suppress infection following IFN treatment (Figure S1A). The screen strategy is depicted in Figure 1A. Cas9-expressing T98G cells were independently transduced with lentiviral vectors (LVs) coding the two-halves of the GeCKO library, at a low multiplicity of infection (MOI). Next-generation sequencing showed more than 94% sgRNA coverage for each sub-library (not shown). Cells were pre-treated with type 1 IFN and incubated with VSV-G-pseudotyped, HIV-1 based LVs coding for an antibiotic resistance cassette. The cells successfully infected despite the IFN treatment were selected by cell survival in the presence of antibiotics. In order to enrich the population with mutants of interest and to limit the presence of false-positives, two additional rounds of IFN

treatment, infection and selection (with different antibiotics) were performed. As expected, the cells enriched after each round became less refractory to HIV-1 infection following IFN treatment (Figure S1B).

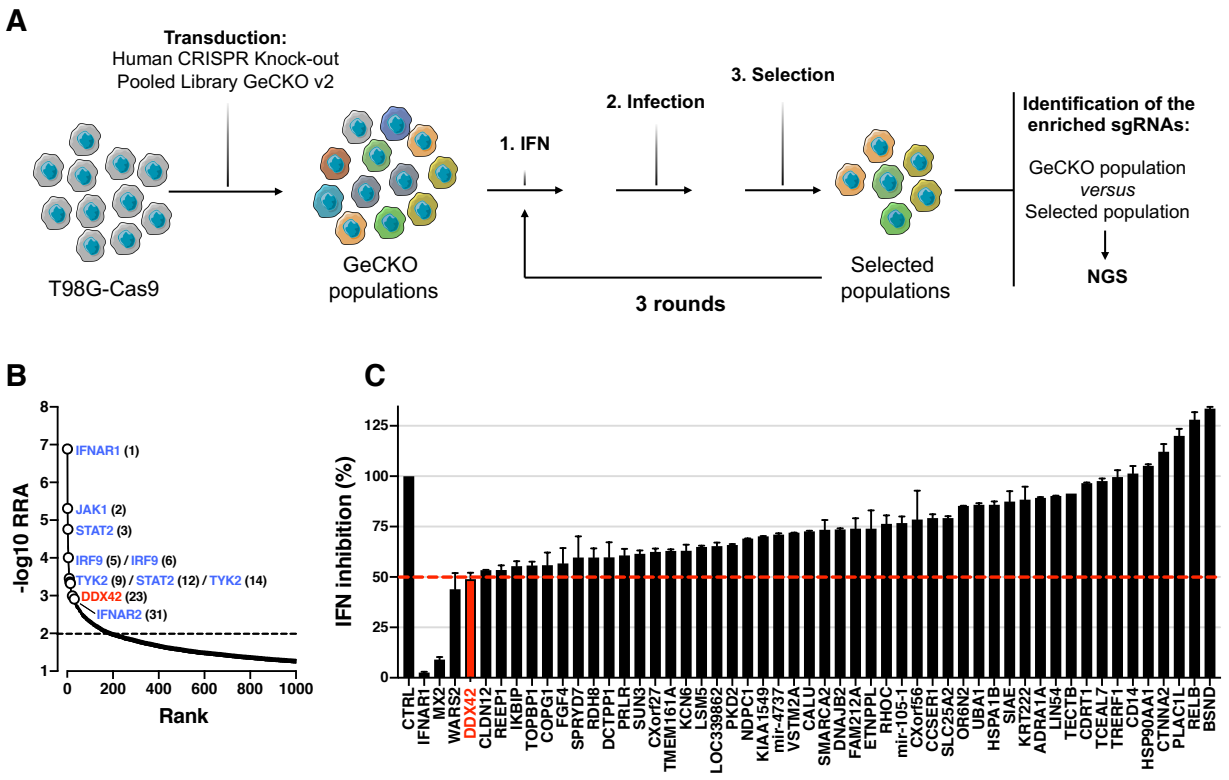

Figure 1. A whole-genome CRISPR/Cas9 screen to identify new HIV-1 inhibitors.

A. Screen strategy. GeCKO cell populations (obtained by transduction of T98G/Cas9 cells with GeCKO v2 LV library) were IFN-treated, challenged with HIV-1 LVs coding an antibiotic resistance gene and selected. Three rounds of IFN treatment, infection and selection were performed. Genomic DNAs of initial GeCKO and 3-time selected populations were extracted, the sgRNA-coding sequences amplified and sequenced.

B. Candidate gene identification. MAGeCK computational statistical tool (Li et al., 2014) was used to establish a Robust Rank Aggregation (RRA) score for each gene based on sgRNA enrichment and number of sgRNAs per gene. Genes belonging to type 1 IFN response pathway (in blue) and DDX42 (in red) are shown (respective ranks into brackets) for 2 independent screens (the results of which were merged in the analysis).

C. Candidate validation. T98G/Cas9/CD4/CXCR4 /Firefly KO populations were generated for the 25 top hits of each screen. The control (CTRL) condition represents the mean of 4 negative CTRL populations, obtained with 4 non-targeting sgRNAs; IFNAR1 and MX2 KO populations were used as positive controls. KO cell populations were treated with IFN and infected with HIV-1 Renilla and luciferase signals were measured 24 h later (Renilla signals were normalized to Firefly). IFN inhibition (i.e. ratio of untreated / IFN-treated conditions) was calculated and set at 100% inhibition for CTRL. A representative experiment is shown (mean and standard deviation from technical duplicates).

The differential sgRNA abundance between the initial GeCKO populations and selected populations was analysed by next-generation sequencing (NGS) and the MAGeCK algorithm was used to rank the gene candidates (Figure 1B). An enrichment was observed for 200 genes (RRA score > 0,01), with the best hits being *IFNAR1*, *JAK1* and *STAT2* (Figure 1B). The crucial mediators of type 1 IFN signalling cascade were among the top hits in both screens (with the notable exception of *STAT1*), validating our approach and confirming the identification of relevant genes. Interestingly, most of the other candidates displayed unknown functions, or functions that were *a priori* unrelated to innate immunity. Of note, very little overlap was observed between the two independent screens, performed with two sub-libraries. However, such a poor overlap between biological replicates does not preclude obtaining valid data (Doench, 2018). The top 25 candidate genes from each screen were selected for further validation. T98G/Cas9 cells expressing HIV-1 CD4 and CXCR4 receptors, as well as firefly luciferase as an internal control (T98G/Cas9/CD4/CXCR4/Firefly cells), were transduced with sgRNA-expressing LVs to generate individual KO populations, using the identified sgRNA sequences. Four irrelevant, non-targeting sgRNAs, as well as sgRNAs targeting *IFNAR1* and *MX2*, were used to generate negative and positive control populations, respectively. The KO cell populations were pre-treated with IFN and infected with an HIV-1 reporter virus expressing Renilla luciferase reporter and bearing HIV-1 envelope (hereafter called HIV-1 Renilla). Infection efficiency was analysed 30 h later (Figure 1C). As expected, IFNAR1 and MX2 KO fully and partially rescued HIV-1 infection from the protective effect of IFN, respectively (Goujon et al., 2013a; Bulli et al., 2016; Xu et al., 2018). The KO of two candidate genes, namely *WARS2* and *DDX42*, allowed a partial rescue of HIV-1 infection from the IFN-induced inhibition, suggesting a potential role of these candidate genes.

DDX42 is a member of the DExD/H box family of RNA helicases, with RNA chaperone activities (Uhlmann-Schiffler et al., 2006) and, as such, retained our attention. Indeed, DEAD box helicases are well-known to regulate HIV-1 life cycle (Taschuk and Cherry, 2020). However, to our knowledge, the impact of DDX42 on HIV-1 replication had never been studied. In order to validate the effect of DDX42 KO on HIV-1 infection in another model cell line, two additional sgRNAs were

designed (sgRNA-2 and -3) and used in parallel to the one identified in the GeCKO screen (sgDDX42-1) (Figure 2A). U87-MG/CD4/CXCR4 cells were used here, as we previously extensively characterized the IFN phenotype in these cells (Goujon et al., 2013a). Control and DDX42 KO cell populations were pre-treated or not with IFN prior to infection HIV-1 Renilla. DDX42 depletion improved HIV-1 infection with all three sgRNAs, confirming that endogenous DDX42 had a negative impact on HIV-1 infection. Interestingly, the increase in infection efficiency induced by DDX42 KO was observed irrespectively of the IFN treatment. DDX42 is not an ISG (Figure S2A and GSE46599 (Goujon et al., 2013a)) but the fact that the IFN-induced state is at least partially saturable (Figure S1A) explains why an intrinsic inhibitor of HIV-1, which is not regulated by IFN, could be identified by our approach. Indeed, removing one barrier to infection presumably rendered the cells more permissive and, in this context, IFN had less of an impact.

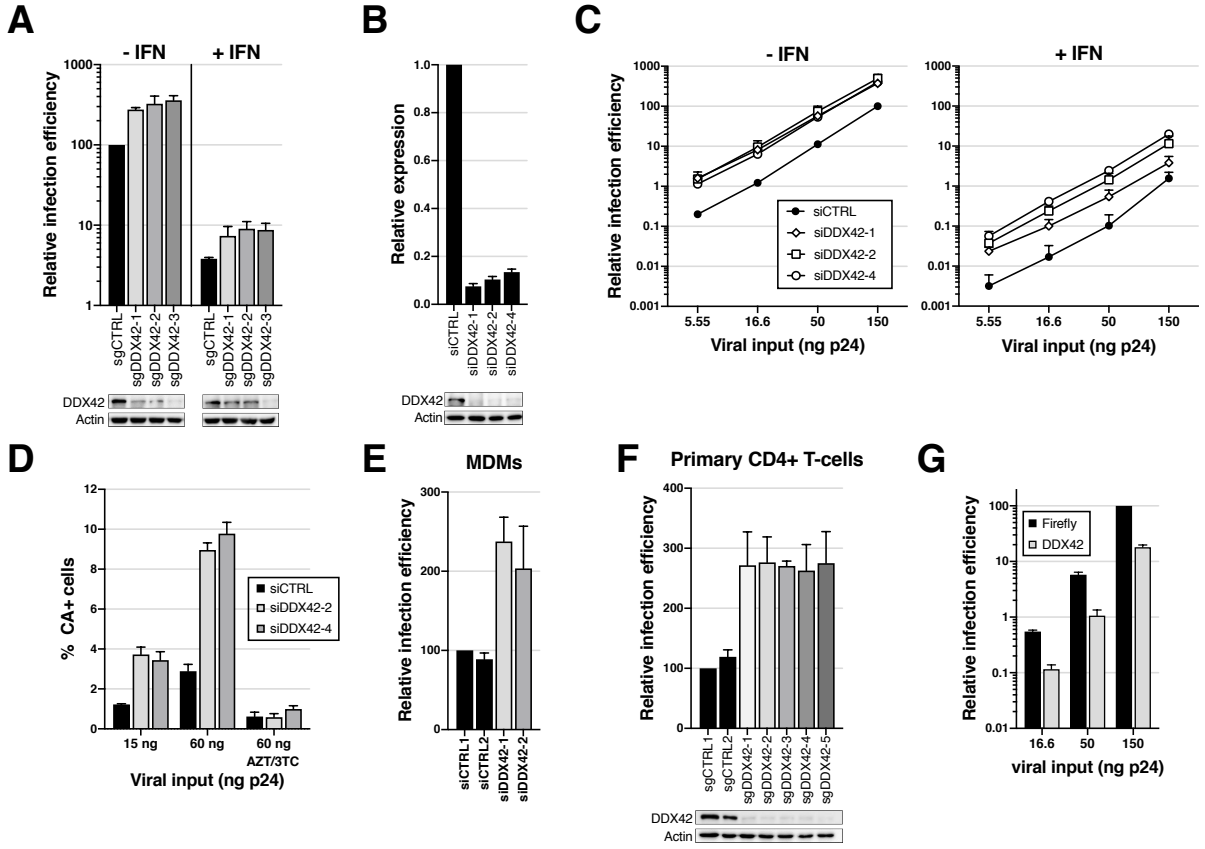

Figure 2. DDX42 is an intrinsic inhibitor of HIV-1.

A. Top: DDX42 KO and CTRL KO U87-MG/CD4/CXCR4/Cas9/Firefly cells were generated using 3 sgRNAs and 4 non-targeting sgRNAs, respectively (for CTRL, the average of data obtained with 4 cell populations is shown). Cells were treated or not with IFN 24 h prior to infection with HIV-1 Renilla. Relative luminescence results for

IFN-treated and -untreated conditions are shown. Bottom: Immunoblot analysis of DDX42 levels is shown for 1 CTRL and DDX42-depleted populations; Actin served as a loading control.

B. DDX42 silencing efficiency measured by RT-qPCR and immunoblot in parallel samples from C.

C. siRNA-transfected U87-MG/CD4/CXCR4 cells were treated or not with IFN for 24 h prior to infection with HIV-1 Renilla. Relative luminescence results for IFN-treated and -untreated conditions are shown.

D. DDX42-depleted cells were infected with HIV-1, and infection efficiency was measured by $p24^{Gag}$ intracellular staining and FACS analysis. When indicated, cells were treated with azidothymidine (AZT) and lamivudine (3TC).

E. siRNA-transfected MDMs were infected with a CCR5-tropic version of HIV-1 Renilla. Relative luminescence results from independent experiments performed with cells from 3 donors are shown.

F. Primary CD4+ T cells were electroporated with Cas9-sgRNA RNPs using 2 non-targeting sgRNAs (sgCTRL1 and 2) and 5 sgRNAs targeting DDX42. Cells were then infected with HIV-1 Renilla and relative infection efficiencies obtained with cells from three donors are shown. DDX42 protein levels were determined by immunoblot, Actin served as a loading control (a representative immunoblot is shown).

G. Firefly- or DDX42-expresssing U87-MG/CD4/CXCR4 cells were infected with HIV-1 Renilla. Relative infection efficiencies are shown.

A-G Data represent the mean ± S.E.M of three independent experiments.

In order to confirm DDX42's effect on HIV-1 infection with an independent approach, we used 3 different siRNAs to knockdown DDX42 expression. We observed that depleting DDX42 (with ~90% efficiency both at the mRNA and protein levels, Figure 2B) increased HIV-1 Renilla infection efficiency by 3 to 8-fold in U87-MG/CD4/CXCR4 cells, irrespectively of the presence of IFN (Figure 2C). Of note, wild-type HIV-1 infection was also impacted by DDX42 silencing, as shown by Capsid ($p24^{Gag}$) intracellular staining 30h post-infection (Figure 2D). We then investigated whether DDX42 had an impact in HIV-1 primary target cells. In monocyte-derived macrophages (MDMs), we observed that HIV-1 infection was increased by about 2-fold following DDX42 silencing (Figure 2E), whereas DDX42 mRNA abundance was decreased by only 40% (Figure S2B). Electroporation of pre-assembled Cas9-sgRNA ribonucleoprotein complexes (RNPs) was used to efficiently deplete DDX42 in primary CD4+ T cells (Figure 2F). DDX42 depletion increased HIV-1 infection by 2- to 3-fold, showing a role of DDX42 as an intrinsic inhibitor of HIV-1 in primary CD4+ T cells. We next analysed the consequences of DDX42 overexpression on HIV-1 infection. An irrelevant control (Firefly) or DDX42 were ectopically expressed in U87-MG/CD4/CXCR4 and the cells were challenged with HIV-1 (Figure 2G). DDX42 overexpression induced a substantial inhibition of HIV-1 infection (~5-fold decrease in infection efficiency in comparison to the control).

Interestingly, the expression of K303E DDX42 mutant, which is unable to hydrolyse ATP and may supposedly act as a dominant negative (Granneman et al., 2006; Rocak, 2005), increased HIV-1 infection by 3-fold, reminiscent of the impact of DDX42 depletion (Figure S2C). Altogether, these data showed that endogenous DDX42 is able to intrinsically inhibit HIV-1 infection.

In order to determine the step of HIV-1 life cycle affected by DDX42, we quantified HIV-1 DNA accumulation over time in DDX42-silenced and control cells (Figure 3A; silencing efficiency is shown in Figure 3B). DDX42 depletion increased accumulation of early and late reverse transcript products (by 2.5- to 8-fold), as well as proviral DNA and 2-long terminal repeat (2-LTR) circles at 48h post-infection (by 2.5- to 4.5-fold). Importantly, DDX42 silencing did not impact HIV-1 entry (Figure S3A). These data suggested that DDX42 could inhibit reverse transcription and/or impact genome stability, leading to a decrease in viral DNA accumulation. We hypothesized that if that was the case, DDX42 should be found in close proximity to HIV-1 reverse transcription complexes during infection. In agreement with this, proximity ligation assay (PLA) performed on HIV-1 infected MDMs showed that DDX42 could indeed be found in close vicinity of Capsid (Figure 3C).

We next examined the ability of DDX42 to inhibit infection by various primate lentiviruses, including lab-adapted strains of HIV-1 (NL4-3, IIIB), transmitted/founders (CH077.t, CH106.c, REJO.c), HIV-2 and simian immunodeficiency virus from rhesus macaque (SIV_{MAC}). DDX42 was depleted or not in TZM-bl reporter cells prior to infection with VSV-G-pseudotyped lentiviruses, and infection efficiency was monitored 24h later (Figure 3D-E). DDX42 depletion increased infection levels similarly with all the tested strains of HIV-1 (i.e. 3- to 5-fold). HIV-2rod10 and SIV_{MAC} infection efficiencies were also slightly improved in the absence of DDX42 (~2-fold). The analysis was then extended to non-primate lentiviruses, equine infectious anemia virus (EIAV) and feline immunodeficiency virus (FIV), using GFP-coding LVs (Figure S3B). DDX42 depletion appeared to increase HIV-1, HIV-2 and FIV LV infection to the same extent (~2-fold), whereas EIAV infection was less impacted. Of note, DDX42 antiviral activity appeared less potent on HIV-1 LVs compared to full-length HIV-1, which might suggest that genome length or cis-acting

elements could play a role in DDX42 inhibition. We also observed that DDX42 depletion led to an increase in infection with GFP-coding, murine leukemia virus (MLV)-derived vectors (Figure 3F). These results strongly support a general antiviral activity of DDX42 against retroviruses.

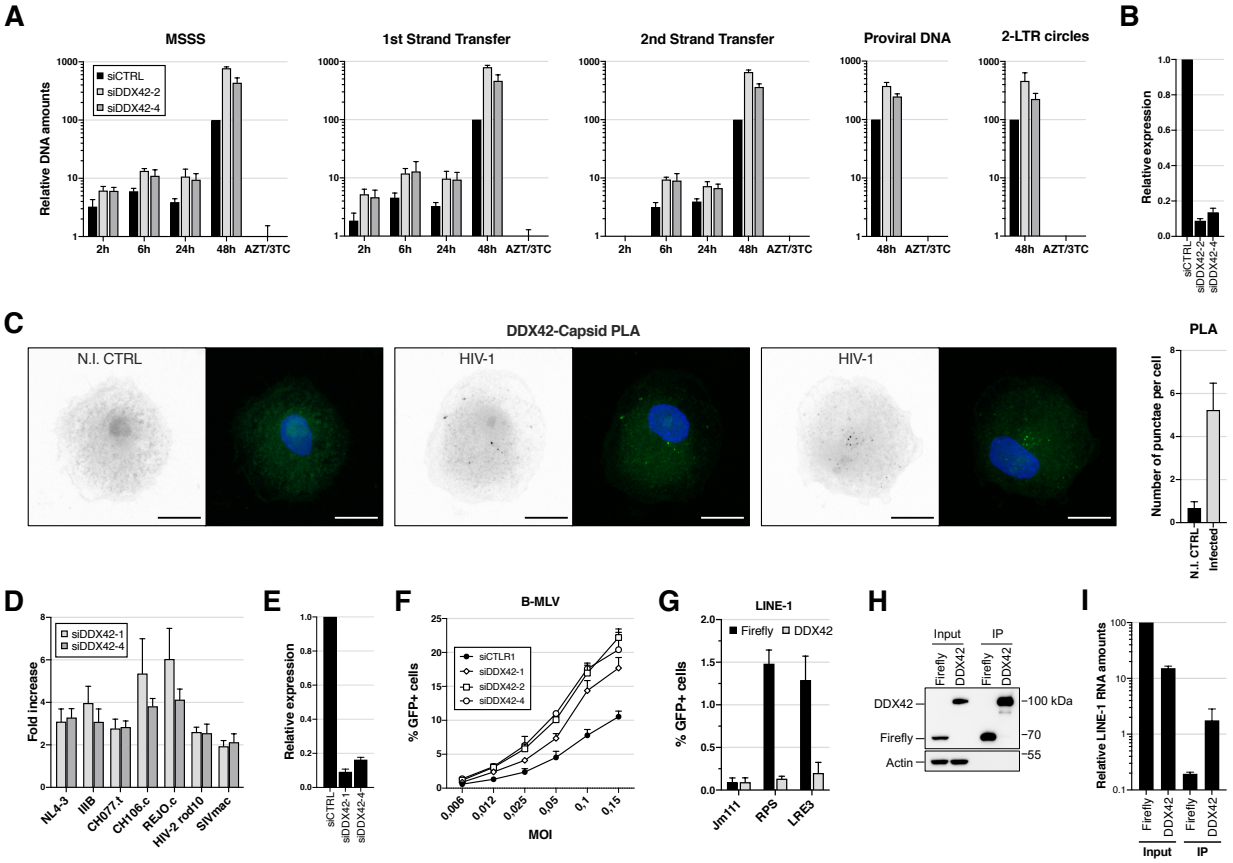

Figure 3. Characterization of DDX42 inhibitory activity against retroviruses and retroelements.

A. siRNA-transfected U87-MG/CD4/CXCR4 cells were infected with HIV-1 and relative amounts of Minus Strand Strong Stop (MSSS), 1st and 2nd Strand Transfer DNAs, and nuclear forms of HIV-1 DNA (proviral DNA, and 2-LTR circles) were quantified by qPCR. DNAs from cells infected for 48 h in the presence of AZT and 3TC were used as a control.

B. Silencing efficiency in parallel samples from A.

C. PLAs were performed in MDMs infected with HIV-1 or not (N.I. CTRL), using anti-Capsid and anti-DDX42 antibodies (nuclei stained with Hoechst). Images were acquired using a LSM880 Airyscan microscope. Left: representative images, scale-bar: 10 μm. Right: Average punctae quantified per cell in 3 independent assays done on MDMs from different donors with mean ± SEM (n>65 cells per condition).

D. siRNA-transfected TZM-bl cells were infected and β-galactosidase signals measured 24 h later. The ratio of the signal in DDX42-depleted versus CTRL cells is shown.

E. Silencing efficiency in parallel samples from D.

F. siRNA-transfected U87-MG/CD4/CXCR4 cells were infected with GFP-coding B-MLV and infection efficiency measured 24h later by FACS.

G. HEK293T were co-transfected with GFP-coding LINE-1 plasmids (RPS-GFP or LRE3-GFP) or with an inactive LINE-1 plasmid (JM111) together with either a Firefly- or DDX42-coding plasmid. GFP expression was measured by FACS 7 days later.
H. HEK293T were co-transfected with pRPS-GFP and a Flag-Firefly- or Flag-DDX42-coding plasmid, followed by Flag immunoprecipitation and immunoblot analysis.
I. RNA extraction and LINE-1 RT-qPCR on parallel samples from H.
Data represent the mean ± S.E.M of 3 (A-G) or 2 (H) independent experiments.

DDX42 can be found in the cytoplasm but is predominantly located in the nucleus (Figure S3D; Uhlmann-Schiffler et al., 2009; Zyner et al., 2019). Considering that DDX42 showed a broad activity against retroviruses and seemed to act at the level of reverse transcription, we sought to investigate whether DDX42 could inhibit retrotransposons. Long interspersed nuclear elements (LINE)-1 are non-LTR retrotransposons, which have been found to be active in the germ line and some somatic cells (Faulkner and Billon, 2018). Interestingly, DDX42 was identified among the suppressors of LINE-1 retrotransposition through a genome-wide screen in K562 cells, although not further characterized (Liu et al., 2018). To confirm that DDX42 could inhibit LINE-1 retrotransposition, HEK293T cells were co-transfected with GFP-expressing LINE-1 plasmids (RPS or LRE3) or an inactive LINE-1 (JM111) together with a DDX42- or a control (Firefly)-expressing plasmid (Moran et al., 1996). LINE-1 retrotransposition was quantified by FACS 7 days later (Figure 3G). As the GFP cassette is cloned in antisense and disrupted by an intron, GFP is only expressed after LINE-1 transcription, splicing, Orf2p-mediated reverse transcription, and integration (Moran et al., 1996). Successful retrotransposition events were observed in >1.25% of CTRL cells, but in only <0.25% of DDX42-expressing cells (i.e. a percentage similar to what observed with the non-active LINE-1), showing that DDX42 ectopic expression suppressed LINE-1 retrotransposition. Next, we investigated whether DDX42 could physically interact with LINE-1 RNAs. Cells were co-transfected with RPS and either flag-tagged-Firefly or -DDX42, the flagged proteins immunoprecipitated, and the proteins and associated RNAs were analysed by immunoblot and RNA extraction and RT-qPCR, respectively (Figure 3H-I). DDX42 expression decreased the total amount of LINE-1 RNAs but an enrichment of LINE-1 RNAs was observed with DDX42 immunoprecipitation.

Finally, we sought to determine whether DDX42's inhibitory activity was specific towards retroviruses and retroelements, or could be extended to other viruses. To this aim, we tested the impact of DDX42 depletion on RNA viruses from 5 different families: the orthomyxovirus influenza A virus (IAV), the rhabdovirus vesicular stomatitis virus (VSV), the alphavirus CHIKV, the flavivirus Zika virus (ZIKV), and the coronavirus SARS-CoV-2, which is responsible for the current coronavirus disease (COVID)-19 pandemic (Figure 4). Strikingly, DDX42 depletion had no impact on IAV or VSV replication (Figure 4A-B), thereby confirming that manipulating DDX42 expression did not have a broad and unspecific impact on target cells. However, depletion of endogenous DDX42 increased infection with ZIKV (Figure 4C), CHIKV and SARS-CoV-2, with a particularly high impact on the latter two (up to 1 log and 3 log increase in infection efficiency with CHIKV and SARS-CoV-2, respectively, Figure 4D and F-G; silencing efficiencies are shown in Figure 4E and H). Plaque assays confirmed a strong impact of DDX42 depletion on infectious SARS-CoV-2 production (Figure 4G). In agreement with this, DDX42 was recently identified as a potential inhibitor of SARS-CoV-2 replication in a CRISPR screen in simian cells (Wei et al., 2020). Next, we used PLA to determine whether DDX42 was in the vicinity of viral components in infected cells. To this aim, PLA was performed with either anti-double strand (ds)RNA or anti-Nucleoprotein (N) antibody, together with anti-DDX42 antibody, followed by an immunofluorescence staining to identify the infected cells (Figure 4I-J). In the latter, there was a higher number of dsRNA-DDX42 and N-DDX42 PLA punctae than in control cells. This strongly suggested an interaction between DDX42 and SARS-CoV-2 viral components.

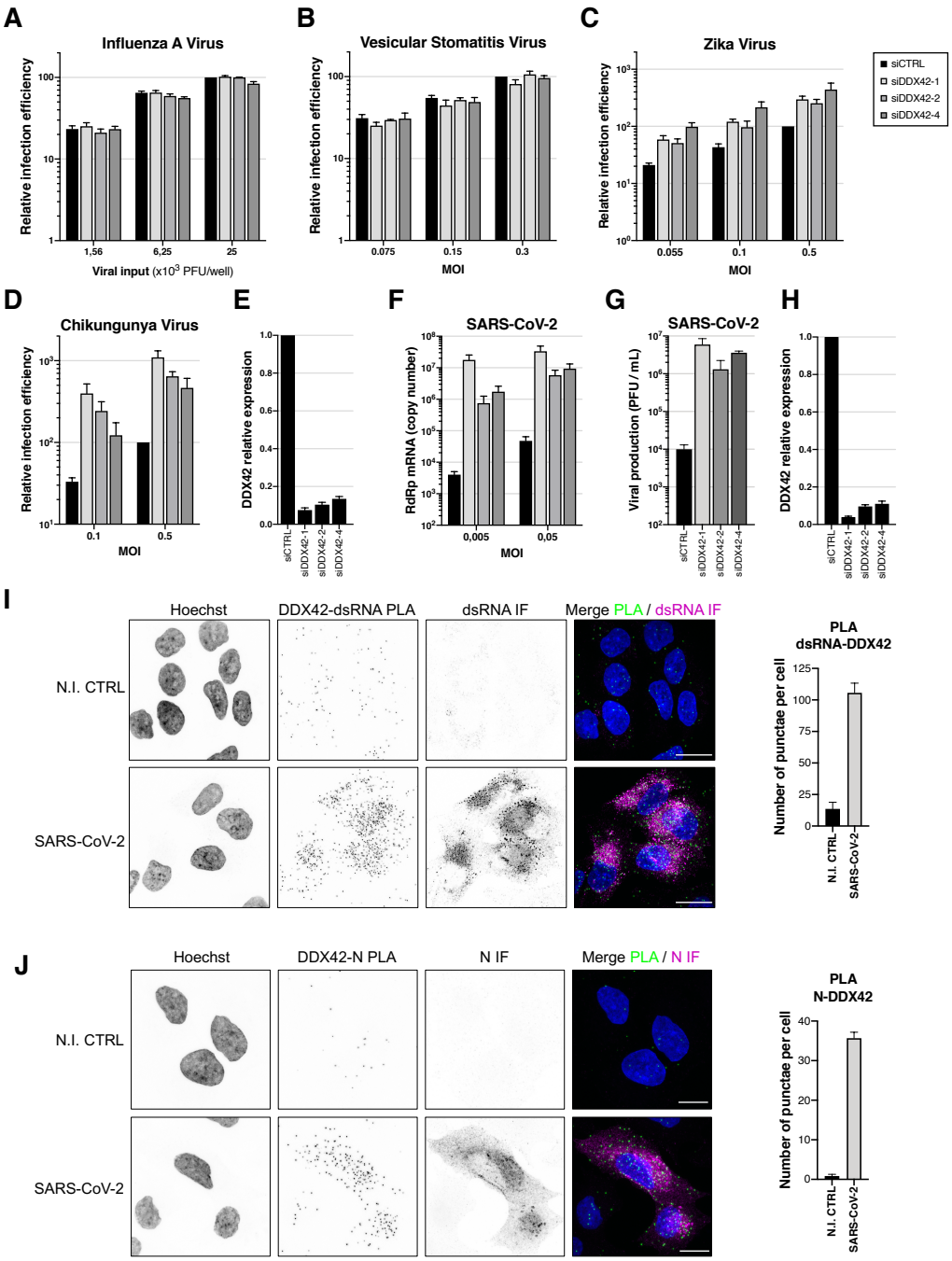

Figure 4. DDX42 exerts a broad antiviral activity.

A. Relative IAV infection efficiency in siRNA-transfected U87-MG cells (Nanoluciferase activity 16 h post infection).

B. Relative VSV infection efficiency in siRNA-transfected U87-MG cells (Firefly activity 24 h post infection).

C. Relative ZIKV infection efficiency in siRNA-transfected U87-MG cells (Nanoluciferase activity 24 h post infection).

D. Relative CHIKV infection efficiency in siRNA-transfected U87-MG cells (Nanoluciferase activity 24 h post infection).

E. Quantification of DDX42 silencing efficiency by RT-qPCR in parallel samples from A-D

F. Relative SARS-CoV-2 infection in siRNA-transfected A549-ACE2 cells (RdRp RT-qPCR 48 h post-infection).

G. Viral production in cell supernatants from F measured by plaque assays.

H. Quantification of DDX42 silencing efficiency in parallel samples from F.

I. A549-ACE2 cells were infected or not with SARS-CoV-2 for 24 h prior to PLA using mouse anti-dsRNA (J2) and rabbit anti-DDX42 antibodies, followed by additional immunofluorescence (IF) staining with anti-mouse Alexa Fluor 546 antibody (PLA in green, IF in magenta). Representative Z-stack projection images are shown; scale bar: 15 μm. Average punctae were quantified in 3 independent PLA assays with mean ± SEM (n>65 cells per condition).

J. Identical to I but using an anti-N antibody instead of anti-dsRNA antibody.

Data represent the mean ± S.E.M. of three (**A-E, I-J**), four (**F, H**) or two (**G**) independent experiments.

Here, we identified for the first time the RNA helicase DDX42 as an intrinsic inhibitor of HIV-1, capable of limiting the efficiency of viral DNA accumulation. Moreover, our study revealed broad activity of endogenous DDX42 against retroviruses and retroelements, which was observed in various cell types, including primary CD4+ T cells. Strikingly, we observed that DDX42 was able to inhibit viruses from other families, which possess different replication strategies, including SARS-CoV-2 and CHIKV. However, DDX42 did not have an impact on all the viruses we tested, reminiscent of broad-spectrum antiviral inhibitors such as MxA, which show some specificity (Haller et al., 2015). Further work is now warranted to explore in depth the breadth of DDX42 antiviral activity and determine whether it is specific of positive RNA viruses.

Interestingly, our PLA assays showed a close proximity between DDX42 and HIV-1 Capsid, which is a viral protein recently shown to remain associated with reverse transcription complexes until proviral DNA integration in the nucleus (Burdick et al., 2020; Dharan et al., 2020; Peng et al., 2014). We also observed a close proximity between DDX42 and SARS-CoV-2 N or dsRNA. Furthermore, LINE-1 RNAs were specifically pulled-down when DDX42 was immunoprecipitated. Taken together, these observations strongly suggest a direct mode of action of DDX42 on viral ribonucleoprotein (RNP) complexes. DDX42 is known to be a non-processive helicase, which also possesses RNA annealing activities and the ability to displace RNA-binding proteins from single-stranded RNAs (Uhlmann-Schiffler et al., 2006). Moreover, DDX42 binds G-quadruplexes (Zyner et al., 2019), which are secondary structures found in cellular and viral nucleic acids and involved in various processes, such as transcription, translation and replication (Fay et al., 2017; Ruggiero and Richter, 2018). All these known activities of DDX42 would be consistent with a

potential role in RNP remodeling (Uhlmann-Schiffler et al., 2006; Will et al., 2002). Nonetheless, further investigation will be needed to determine whether DDX42 acts directly by altering viral RNPs, and, if that's the case, what are the determinants for viral RNP recognition.

In conclusion, this work highlights the importance of understanding the mechanism of action of DDX42 RNA helicase and its contribution to the control of RNA virus replication, an understanding which may contribute to the development of future antiviral interventional strategies.

Methods

Plasmids. The pLentiCas9-Blast, pLentiGuide-Puro vectors and the GeCKO sub-library A and B plasmids were a gift from Prof. F. Zhang (Addgene #52962, #52963, and #1000000048, respectively (Sanjana et al., 2014)). LVs coding for sgRNAs targeting the candidate genes and control genes were obtained by cloning annealed oligonucleotides in BsmBI-digested pLentiGuide-Puro, as described (Addgene). Control sgRNAs and sgRNAs targeting the candidate genes, *MX2* and *IFNAR1*, were designed with the Optimized CRISPR Design tool (not available anymore), or with Chopchop (chopchop.cbu.uib.no). The sgRNA coding sequences used were as follow: MX2 5'-CCGCCATTCGGCACAGTGCC-3', IFNAR1 5'-GACCCTAGTGCTCGTCGCCG-3', sgCTRL-1 5'-AGCACGTAATGTCCGTGGAT-3', sgCTRL-2 5'-CAATCGGCGACGTTTTAAAT-3', sgCTRL-3 5'-TTAATTTGGGTGGGCCCTGC-3', sgCTRL-4 5'-TTGGATATTAATTAGACATG-3', sgDDX42-1 5'-TCCTGAACCACACCAGCAGT-3', sgDDX42-2 5'-GGTGGTCCTGGCACTAAGCG-3', sgDDX42-3 5'-AGGCACTGTGGGACTGCTGT-3'.All the other sgRNA sequences are available upon request. In order to produce the HIV-1 based LVs used to perform the different steps of the screen (pRRL.sin.cPPT.CMV/NeomycinR.WPRE, pRRL.sin.cPPT.CMV/HygromycinR.WPRE and pRRL.sin.cPPT.CMV/ZeocinR.WPRE), neomycin, hygromycin and zeocin resistance genes (i.e. the genes coding for Neomycin phosphotransferase II, Hygromycin B phosphotransferase, and *Sh ble*) were amplified by PCR from pcDNA3.1 (ThermoFisher Scientific), pAHM (Goujon et al., 2013a), and pcDNA3.1/Zeo (ThermoFisher Scientific), respectively, and cloned by replacement of GFP in pRRL.sin.cPPT.CMV/GFP.WPRE (Goujon et al., 2008) using BamHI and SalI restriction sites. The pRRL.sin.cPPT.SFFV/E2-crimson-IRES-PuromycinR.WPRE has been described (Doyle et al., 2018). Human DDX42 cDNA was amplified by RT-PCR using the SuperScript III™ (Invitrogen) from mRNAs of MDMs and cloned by replacement of the enhanced E2-crimson in BamHI-XhoI-digested pRRL.sin.cPPT.SFFV/E2crimson-IRES-PuromycinR.WPRE, in order to obtain pRRL.sin.cPPT.SFFV/DDX42-IRES-PuromycinR.WPRE. The pRRL.sin.cPPT.SFFV/CD4-IRES-CXCR4.WPRE was obtained by replacement of E2-

crimson-IRES-PuroR in pRRL.sin.cPPT.SFFV/E2-crimson-IRES-PuromycinR.WPRE with a BamHI/SalI fragment digested CD4-IRES-CXCR4 PCR fragment obtained from pMLV-CD4-IRES-CXCR4 (a gift from Prof. N. Sherer, Wisconsin University, USA). pRRL.sin.cPPT.SFFV/Firefly-IRES-PuromycinR.WPRE was obtained by amplification of Firefly by PCR from pGL4 (Promega) and cloned into BamHI-XhoI-digested pRRL.sin.cPPT.SFFV/E2-crimson-IRES-PuromycinR.WPRE. In some experiments, LVs without a selection marker were used: the IRES-PuromycinR cassette was removed by XhoI-SalI digestion and subsequent ligation, to obtain pRRL.sin.cPPT.SFFV/Firefly.WPRE and pRRL.sin.cPPT.SFFV/DDX42.WPRE. Human ACE2 coding sequence (NM_021804) was amplified using the SuperScript® III One-Step RT-PCR System with Platinum® Taq (Invitrogen) from 500 ng RNA obtained from 293T cells, using primers 5'-AATTAATTTAGCGGCCGCATGTCAAGCTCTTCCTGGCTCC-3' and 5'-AATTAATTTACTCGAGCTAAAAGGAGGTCTGAACATCATCAGTG-3, digested and inserted into NotI-XhoI-digested pRRL.sin.cPPT.SFFV/.WPRE to generate pRRL.sin.cPPT.SFFV/ACE2.WPRE (Addgene 145842). Flag-DDX42 and Flag-Firefly were amplified by PCR from the aforementioned LV plasmids and cloned into a NotI-XhoI-digested modified version of pCAGGS (Moncorge et al., 2013) to obtain pCAGGS/flag-DDX42.WPRE and pCAGGS/flag-Firefly.WPRE. The NL4-3/Nef–internal ribosome entry signal (IRES)-Renilla (NL4-3/Nef-IRES-Renilla) and the CCR5-version of this proviral clone were gifts from Prof. Sumit Chanda (Goujon et al., 2013b). Wild-type and Ba-L Env bearing HIV-1 NL4-3, IIIB and HIV-2 proviral clones have been described (Adachi et al., 1986; Simon et al., 1995; Schaller et al., 2011), as well as the transmitted founder HIV-1 molecular clones CH077.t, CH106.c, REJO.c (gifts from Prof. B. Hahn, (Ochsenbauer et al., 2012)) and HIV-2_{ROD10} and SIV_{MAC239} (Ryan-Graham and Peden, 1995; Gaddis et al., 2004). GFP-coding HIV-1 based LV system (i.e. p8.91 HIV-1 Gag-Pol, pMD.G, and GFP-coding minigenome), and HIV-2, FIV, and EIAV-derived, GFP coding LVs, as well as MLV-derived, GFP coding retroviral vectors have all been described (Naldini et al., 1996; Bainbridge et al., 2001), (O'Rourke et al., 2002; Saenz et al., 2005). The LINE-1 plasmid 99 RPS-GFP PUR (pRPS-GFP), 99 RPS-GFP JM111 PUR (pJM111) and pLRE3-GFP were developed by Prof. Kazazian's lab (Moran et al., 1996; Ostertag et al., 2000; Goodier et al., 2012).

Cell lines. Human cell lines HEK293T, U87-MG, TZM-bl were obtained from the ATCC and the AIDS reagent program, respectively. T98G cells were a gift from Prof. G. Kochs (Freiburg University, Germany), A549 and MDCK cells were a gift from Prof. W. Barclay (Imperial College London, UK), Vero E6 cells were a gift from Christine Chable (CEMIPAI, CNRS). These cell lines were cultured in Dulbecco's Modified Eagle Medium (DMEM) supplemented with 10% fetal bovine serum and 1 % penicillin-streptomycin (Thermofisher). T98G/Cas9 and U87-MG/Cas9 were obtained by transduction of T98G and U87-MG, respectively, with HIV-1-based LVs expressing the spCas9-P2A-Blasticidin cassette (pLentiCas9-Blast (Sanjana et al., 2014)). U87-MG/CD4/CXCR4 have been described (Goujon et al., 2013a) and were further modified to express Cas9 and Firefly using pLentiCas9-Blast and pRRL.sin.cPPT.SFFV/Firefly.WPRE, respectively. T98G/Cas9/CD4/CXCR4/Firefly were obtained by successive transductions of T98G/Cas9 with pRRL.sin.cPPT.SFFV/CD4-IRES-CXCR4.WPRE at a high MOI, and pRRL.sin.cPPT.SFFV/Firefly.WPRE, at a low MOI, respectively. Cell surface staining with anti-CD4 and CXCR4 antibodies (Miltenyi Biotec) confirmed than more than 95% cells were positive for both markers. A549 cells stably expressing ACE2 were generated by transduction with RRL.sin.cPPT.SFFV.ACE2.WPRE containing-vector.

For antibiotic selection, cells were treated with 10 μg/mL Blasticidin (InvivoGen), 1 mg/mL Zeocin (InvivoGen), 2 μg/mL Puromycin (Sigma-Aldrich), 250 μg/mL Hygromycin (Sigma-Aldrich), 1 mg/mL G418 (Sigma-Aldrich). When indicated, IFN (universal type 1 IFN, PBL Interferon Source) was added at 1000 U/mL for 16-24h prior to virus infection or RNA extraction, and AZT and 3TC (AIDS reagent program) at 10 μM for 2 h prior to infection.

Primary cells. Blood from healthy donors was obtained from the Etablissement Français du Sang, under agreement n°21PLER2019-0106. Peripheral blood mononuclear cells (PBMCs) were isolated by centrifugation through a Ficoll® Paque Plus cushion (Sigma-Aldrich). Primary human CD4+ T cells and monocytes were purified by positive selection using CD3 and CD14

MicroBeads, respectively (Miltenyi Biotec), as previously described (Goujon et al., 2013a). Monocytes were incubated for 3 hours in serum-free Roswell Park Memorial Institute (RPMI) 1640 medium and further differentiated into macrophages by culture for 5-7 days in RPMI 1640 supplemented with 10% fetal calf serum, 1% penicillin-streptomycin and 100 ng/ml granulocyte-macrophage colony-stimulating factor (GM-CSF; Miltenyi). CD4+ T cells were in cultures in RPMI supplemented with 10% fetal bovine serum and 1% penicillin-streptomycin and stimulated 48h with 10 µg/ml phytohemagglutinin (PHA) (Fisher Scientific) and 50 U/mL interleukin-2 (IL-2, Miltney Biotec) prior to electroporation.

Genome-scale CRISPR/Cas9 screens. The plasmids coding GeCKO sub-libraries A and B were amplified and prepared according to the provided guidelines (Lentiviral Crispr Toolbox, Addgene). 60 million T98G/Cas9 cells were transduced with GeCKO LVs at a MOI of 0,1 to cover about 100-times the half-library complexity. After 48h, the cells were selected with puromycin, amplified for 12-15 days. 45 million cells were harvested and frozen down at -80°C for subsequent genomic DNA extraction, using the QIAamp DNA Blood Maxi Kit according to manufacturer's instructions (Qiagen). In parallel, 60 million cells from the initial GeCKO populations were used for the screen. The cells were treated with 1000 U/mL IFN for 24h, infected with LVs coding a hygromycin resistance cassette. 48h later the cells selected with hygromycin and the surviving cells amplified. Two other rounds of IFN treatment, LV infection and antibiotic selection were subsequently performed with LVs coding a neomycin resistance cassette and a zeocin resistance cassette, respectively. The three time-selected populations were amplified and 45 million cells were harvested and stored at -80°C for subsequent genomic DNA extraction, as previously. After genomic DNA extraction, the sgRNA coding sequences integrated in the genomic DNA from the initial and 3-times selected populations were amplified by touch-down PCR and sequenced by Illumina deep sequencing. To this aim, 120 µg of genomic DNA was amplified using DNA Herculase II Fusion DNA polymerase (Agilent) in the presence of 2% DMSO, 1 mM of dNTPs; and 400 nM of the following primers: Forward-primer1: 5'-TCGTCGGCAGCGTCAGATGTGTATAAGAGACAGCTTGTGGAAAGGACGAAACACC-3' for

screen A or Forward_primer2: 5'-TCGTCGGCAGCGTCAGATGTGTATAAGAGACAGGATCTTGTGGAAAGGACGAAACACC-3' used for screen B, together with reverse primer: 5'-GTCTCGTGGGCTCGGAGATGTGTATAAGAGACAAAGGTCCATTAGCTGCAAAGATTCCTCTC-3'). Briefly, after 5 minutes at 95°C, 14 cycles of pre-amplification were performed with a hybridization temperature decreasing by 0.5°C per cycle (30 sec at 95°C, 30 sec at 60°C, 30 sec at 72°C), followed by 30 cycles of amplification (30 sec at 95°C, 30 sec at 53°C, 30 sec at 72°C). 50 ng of each amplicon was dual indexed in a 5-cycle PCR reaction using the PCR module and indexed primers from the Nextera kit (Illumina). Resulting libraries were purified on AMPure XP magnetic beads (Beckman Coulter) using a 0,8X ratio and verified on Fragment Analyzer using the HS NGS fragment kit (Agilent). Libraries were quantified using microfluorimetry (QuBit, Invitrogen), mixed with a PhiX library (Illumina) and sequenced on one single read 50nt lane of Hiseq2500 using the rapid mode.

Image analyses and base calling were performed using the Illumina HiSeq Control Software and Real-Time Analysis component (v1.18.66.3). Demultiplexing was performed using Illumina's conversion software (bcl2fastq 2.20). The quality of the raw data was assessed using FastQC (v0.11.5) from the Babraham Institute and the Illumina software SAV (Sequencing Analysis Viewer). Potential contaminants were investigated with the FastQ Screen (Wingett and Andrews, 2018) (v0.11.4) software from the Babraham Institute.

Sequencing reads were trimmed using Cutadapt (Martin, 2011) (v1.13), with options -g [primer sequence] -u [length of remaining 3' bases] -e 0.2 -m 18 -l 20, to remove primer sequences and retrieve the 20 bases long sequences corresponding to sgRNAs. These retrieved sequences were then aligned to the GecKOv2 Human Library (A or B) reference sequences (keeping only non-duplicated sgRNA sequences, the duplicated ones being annotated) using Bowtie (Langmead et al., 2009) (v1.2), with options -v 2 -norc -S. Resulting bam files were sorted and indexed using Samtools (Li et al., 2009) (v1.5). Quantification of sgRNAs was done using Samtools idxstats. MAGeCK (Li et al., 2014) (v0.5.7) was used to normalize (total count method) and identify

enriched sgRNAs and genes in 3-times selected cell populations versus starting GeCKO transduced cells (mageck test command).

Lentiviral and retroviral production. To produce lentiviral vector particles, HEK293T cells were transfected by polyethylenimine (PEI) co-transfection with miniviral, HIV-1 based genome coding plasmids (e.g. LentiCas9-Blast, LentiGuide-Puro or pRRL-SFFV), p8.91 (HIV-1 GagPol) and pMD.G (VSV-G) at a ratio of 1:1:0.5, respectively. The medium was replaced after 6h and viral particles were harvested 42h later, filtered, and directly used to transduce target cells (or stored at -80°C). After 4 to 6 hours, the transduction medium was replaced with complete DMEM, and the cells were treated 48h later with the relevant antibiotics. The HIV-2-, FIV-, EIAV-GFP coding LVs were produced using GFP-coding HIV-2-, FIV-, EIAV-based miniviral genomes, together with HIV-2-, FIV-, EIAV- GagPol, expression constructs and pMD.G at a ratio of 1:1:0.5. MIGR1 MLV-derived retroviral vectors were obtained with B-MLV Gag-Pol-expressing plasmid pCIG3B, the GFP-expressing minigenome pMIGR1 and pMD.G. at a ratio of 1:1:0.5, respectively and harvested as previously described.

HIV-1 Renilla and NL4-3 HIV-1 were produced by standard PEI transfection of HEK293T. When indicated, pMD.G was cotransfected with the provirus at a 3:1 ratio. The culture medium was changed 6h later, and virus-containing supernatants were harvested 42h later. Viral particles were filtered, purified by ultracentrifugation through a sucrose cushion (25% weight/volume in Tris-NaCl-EDTA buffer) for 75 min at 4°C and 28,000 rpm using a SW 32 TI rotor (Beckman Coulter), resuspended in serum-free RPMI 1640 or DMEM medium and stored in small aliquots at -80°C. Viral particles were titrated using an HIV-1 $p24^{Gag}$ Alpha-Lisa kit and an Envision plate reader (Perkin Elmer) and/or by determining their infection titers on target cells.

Lentiviral and retroviral infections. For infections with replication-competent HIV-1 Renilla or wild-type and/or VSV-G pseudotyped-HIV-1, target cells were plated at 2.5×10^4 cells per well in 96-well plates or at 2×10^5 cells per well in 12-well plates and infected for 24-48 h before lysis and Renilla (and Firefly) luciferase activity measure (Dual-Luciferase® Reporter Assay System

Promega) or fixation with 2% paraformaldehyde (PFA)-PBS, permeabilization (Perm/Wash buffer, BDBiosciences) and intracellular staining with the anti-p24^{Gag} KC57-FITC antibody (Beckman Coulter), as described previously (Goujon and Malim, 2010). For TZM-bl assays, the β-galactosidase activity was measured using the Galacto-Star™ system (ThermoFisher Scientific). For infections with lentiviral and retroviral vectors, target cells were plated at 2.5 x 10^4 cells per well in 96-well plates the day prior to infection with vectors at the indicated MOIs, and the percentages of infected cells were scored by flow cytometry 24h later. For primary CD4+ T cell infections, 10^5 cells were infected with 100 ng p24^{Gag} of HIV-1 Renilla for 24 h prior to lysis and luciferase activity measure. For MDM infections, 8 x 10^4 cells were infected with 100 ng p24^{Gag} of a CCR5-tropic version of HIV-1 Renilla for 30 h prior to lysis and luciferase activity measure.

Retrotransposon assays. For GFP-based retrotransposon assays, HEK293T cells (2 x 10^5 cells) were co-transfected with either 1 µg of pJM111 (a negative control with two point mutations in ORF1 that abolish retrotransposition), pRPS-GFP or pLRE3-GFP with either 1 µg of pCAGGS-Flag-Firefly or pCAGGS-Flag-DDX42. At 7 days post-transfection, the percentage of GFP-expressing cells was scored by flow cytometry.

CRISPR/Cas9 knock-out

For CRISPR/Cas9 knock-out in cell lines, Lentiguide-Puro LVs coding sgRNAs targeting the indicated genes or non-targeting sgRNAs were produced, and U87-MG Cas9/CD4/CXCR4/Firefly were transduced for 6 h before replacing the supernatants with fresh, complete medium. The transduced cells were selected with puromycin two days later and amplified for 12-15 day. For CRISPR/Cas9 knock-out in activated primary CD4+ T cells, 2 million cells per condition were washed with PBS1X, and electroporated using the 4d-Nucleofector® (Lonza) and the Amaxa P3 primary cell kit with 183 pmol of crispr/tracr RNA duplex (Alt-R CRISPR-Cas9 crRNA XT and tracrRNA XT, IDT®) and 61 pmol of Cas9 (Alt-R® S.p. Cas9 Nuclease V3, IDT®). After electroporation, the cells were incubated for 4 days at 37°C in X-VIVO15 medium (Lonza) supplemented with 1% pen/strep and IL-2 at 500 U/ml prior to cell counting and infection. The

crRNA sequences of the sgDDX42-1, -2, and -3 were identical to the ones cloned in pLentiguide-Puro, and the crRNA of the sgDDX42-4 and sgDDX42-5 were pre-designed by IDT®, as follow: sg4-DDX42 5'-CGGAGATCTATTAACTGCTG-3', sg5-DDX42 5'-GAGTTGGTGAGTTTTCAGC-3'.

siRNA transfection. DDX42 and control knockdowns were achieved by transfecting the indicated siRNAs at 44nM, 14.2nM, and 100nM final in U87-MG cells, TZM-bl cells and MDMs, respectively, with lipofectamine RNAimax (Thermofisher Scientific) according to the manufacturer's instructions. The scramble siRNA controls used were universal siCTRL1 (SIC001) and siCTRL2 (SIC002) (Sigma-Aldrich) and the sequences of the siRNAs targeting DDX42 were siDDX42-1: 5'-CAGAAUGCCUGGUUUCGGA-3' (SASI_Hs01_00119846, Sigma-Aldrich®), siDDX42-2: 5'-CUUACCUUGUGUUUGAUGA-3' (SASI_Hs01_00119845, Sigma-Aldirch®), siDDX42-4: 5'-AUCUCGAAUACCCUUUACG-3' (ID :136410, Ambion®).

RNA immunoprecipitation. HEK293T cells were co-transfected with equal amounts of pRPS-GFP and pCAGGS-Flag-DDX42 or -Flag-Firefly. 4 days post-transfection, cells are washed twice in PBS1X, incubated 10 min with 0,1% formaldehyde in PBS1X and 5 min in 250 mM Glycine and washed twice in cold PBS1X. Cells are lysed in RIPA buffer (50 mM Tris/HCl pH 7.5, 150 mM NaCl, 1% NP-40, 0.5% sodium deoxycholate, 1 mM EDTA, protease inhibitor cocktail and 40 U/mL RNasin). The lysates were clarified by centrifugation at 16,000*g*, for 10 min at 4 °C. Fractions of cell lysates were harvested at this stage to serve as controls for protein and RNA inputs (15%) and the rest was incubated with Flag-magnetic beads (Life Technologies) for 2 h, at 4 °C. The beads were washed 5 times and the immunoprecipitated proteins eluted using 150 µg/mL 3x Flag peptide (Sigma–Aldrich) in elution buffer (50 mM Tris/HCl pH 7.5, 75 mM NaCl, 1mM DTT, protease inhibitor cocktail and 40 U/mL RNasin) for 2 h. Fractions of eluates were harvested for immunoblot analysis (1/6th) and the rest subjected to RNA extraction (5/6th). RNA extractions were performed using TRIzol (ThermoFisher Scientific).

RNA quantification. 0,5-2 x 10^6 cells were collected 2-3 days after siRNA transfection or 24h after IFN treatment or no treatment, and total RNAs were isolated using the RNeasy kit with on-column DNase treatment (Qiagen). cDNAs were generated using 250 ng RNA (High-Capacity cDNA Reverse Transcription Kit, Applied Biosystem, ThermoFisher Scientific, catalogue number 4368814) and analysed by quantitative (q)PCR using TaqMan gene expression assays (Applied Biosystem) specific for *ACTB* (Hs99999903_m1), GAPDH (Hs99999905_m1), and DDX42 (Hs00201296_m1). Triplicate reactions were run according to the manufacturer's instructions using a ViiA 7 Real-Time PCR system. For relative quantification, samples were normalized to both *ACTB* and *GAPDH* mRNA expression and the ΔΔCt analysis.

For the measure of LINE-1 RNAs, 100 ng RNA (or 25 μl of RNA extracted from the IP eluates, i.e. ~60% of the total amount of immunoprecipitated RNA) were reverse transcribed and analysed by qPCR using primers and probe specific for *ORF2*: ORF2-forward 5'-CACCAGTTAGAATGGCAATCATTAAA-3', ORF2-reverse 5'-GGGATGGCTGGGTCAAATGG-3' with ORF2-probe 5'-[FAM]-AGGAAACAACAGGTGCTGGAGAGGATGC-[TAMRA]-3. Absolute quantification was performed using a pRPS-GFP standard curve.

For the measure of SARS-CoV-2 replication, 3 x 10^5 cells were harvested and total RNA was extracted using the RNeasy kit (Qiagen) employing on-column DNase treatment. 125 ng of cellular RNAs were used to generate cDNAs that were analysed by qPCR using RdRp primers and probe, as follow: RdRp_for 5'-GTGARATGGTCATGTGTGGCGG-3', RdRp_rev 5'-CAAATGTTAAAAACACTATTAGCATA-3', and RdRp_probe 5'-[FAM]-CAGGTGGAACCTCATCAGGAGATGC-[TAMRA]-3' (Corman et al., 2020). pRdRp (which contains an RdRp fragment amplified from SARS-CoV-2 infected cell RNAs using primers RdRp_for and RdRp_rev and cloned into pPCR-Blunt II-TOPO) was diluted in 20 ng/ml salmon sperm DNA to generate a standard curve to calculate relative cDNA copy numbers and confirm the assay linearity (detection limit: 10 molecules of RdRp per reaction).

Quantification of HIV-1 DNAs. To measure HIV-1 cDNAs, 2 x 10^5 cells transfected with a control siRNA or siRNAs targeting DDX42 were plated in 24-well plates, and treated or not with 10 μM

AZT and 3TC 1-2 h prior to infection. The cells were infected with NL4-3 HIV-1 (60 ng $p24^{Gag}$) for 2 h at 37°C, washed with PBS1X and incubated in complete DMEM before being harvested at the indicated times. Cell pellets were frozen at -80°C after two washes in PBS1X. Total DNA extraction was performed using the DNeasy kit (Qiagen) according to the manufacturer's instructions, and a DpnI-treatment step was performed prior to qPCR. Strong stop reverse transcription products were detected using forward primer oHC64 5'-TAACTAGGGAACCCACTGC-3' and reverse primer oHC65 5'-GCTAGAGATTTTCCACACTG-3', 2nd strand transfer product using oHC64 and oSA63R 5'-CTGCGTCGAGAGATCTCCTCTGGCT-3', together with oHC66 probe 5'-[FAM]-ACACAACAGACGGGCACACACTA-[TAMRA]-3'. 2-LTR circular forms were detected using 2LTR-forward 5'-GTAACTAGAGATCCCTCAG-3' and 2LTR-reverse 5'-TGGCCCTGGTGTGTAGTTC-3' together with 2LTR-probe 5′-[FAM]-CTACCACACACAAGGCTACTTCCCTGAT-[TAMRA]-3'. Integrated viral DNA was analysed using an Alu qPCR as described before (Goujon et al., 2013a). Briefly, a preamplification of 16 cycles was performed (15 sec at 94°C, 15 sec at 55°C, 100 sec at 68°C) with Platinum Taq DNA High Fidelity polymerase (Invitrogen) using 100 nM of genomic Alu forward primer 5′-GCCTCCCAAAGTGCTGGGATTACAG and 600 nM of U3-reverse primer 5'-CTTCTACCTTATCTGGCTCAAC-3'. The pre-amplification step was performed on serial dilutions of all the DNA samples, as well as of a positive control (total DNA from U87-MG infected with a high input of NL4-3), to ensure the linearity of the assay. Background levels were assessed using linear, one-way amplification by performing the pre-amplification PCR with the U3-reverse primer alone. Then a qPCR was performed on pre-amplification products using U3-forward primer 5'-TCTACCACACACAAGGCTAC-3' and U3-reverse primer with the U3 probe 5'-[FAM]-CAGAACTACACACCAGGGCCAGGGGTCA-[TAMRA]-3'. qPCR reactions were performed in triplicates, in Universal PCR master mix using 900nM each primer and 250nM probe with the following program: 10 min at 95°C followed by 40 cycles (15 sec at 95°C and 1 min at 60°C). pNL4-3 or pTOPO-2LTR (generated by pTOPO cloning of a 2-LTR circle junction amplified from NL4-3 infected cells, using oHC64 and U3-reverse primers into pCR™2.1-TOPO™) were diluted

in 20 ng/ml of salmon sperm DNA to create dilution standards used to quantify relative cDNA copy numbers and confirm the linearity of all assays.

Proximity Ligation assay. The proximity ligation assays were performed using the Duolink® in situ Detection Reagents (Sigma-Aldrich, DUO92014). For PLA with HIV-1, MDMs were plated in 24-well plates with coverslips pre-treated with poly-L-lysin (Sigma-Aldrich) and infected with 1 μg $p24^{Gag}$ of HIV-1 NL4-3 (Ba-L Env) or mock-infected. For PLA with SARS-CoV-2, A549-ACE2 cells were plated in 24-well plates with coverslips and infected at an MOI of 0,1. 24 h later, the cells were fixed with 2-4% paraformaldehyde in PBS1X for 10 min, washed in PBS1X and permeabilized with 0.2% Triton X-100 for 10 min. After a couple of washes in PBS1X, either NGB buffer (50 mM NH_4Cl, 2% goat serum and 2% bovine serum albumin in PBS) or Duolink® blocking solution was added for 1h. Cells were incubated with mouse AG3.0 anti-HIV-1 Capsid antibody (National Institutes of Health (NIH) AIDS Reagent Program #4121), or J2 anti-dsRNA antibody (SCICONS), or anti-SARS-CoV-2 Nucleoprotein (N; BioVision), and rabbit anti-DDX42 antibody (HPA023571, Sigma-Aldrich) diluted in NGB buffer or in Duolink® blocking solution for 1h. After 2 washes in PBS1X, the cells were incubated with the DUOLINK® in situ PLA® Probe Anti-rabbit minus (DUO92006) and DUOLINK® in situ PLA® Probe Anti-mouse plus (DUO92001) for 1h at 37°C. After 2 washes in PBS1X, the ligation mix was added for 30 min at 37°C. After 2 washes in PBS1X, the cells were incubated with the amplification mix for 100 min at 37°C followed by 3 washes in PBS1X. In the case of SARS-CoV-2 infection, an additional staining was performed by incubating cells in an anti-mouse Alexa Fluor secondary antibody. Finally, the cells were washed twice with PBS1X and stained with Hoechst at 1 μg/mL for 5 min, washed again and the coverslips mounted on slides in Prolong mounting media (ThermoFisher Scientific). Z-stack images were acquired using an LSM 880 confocal microscope (ZEISS) using a 63x lens. PLA punctae quantification was performed using the FIJI software (Schindelin et al., 2012). Briefly, maximum z-projections were performed on each z-stack and the number of nuclei per field were quantified. Then, by using a median filter and thresholding, PLA punctae were isolated and quantified automatically using the Analyse Particles function. To obtain a mean number of dots per cell, the

number of PLA dots per field were averaged by the number of nuclei. In the case of SARS-CoV-2 infection, the infected cells were identified using N or dsRNA immunofluorescence staining. For representative images, single cells were imaged using a LSM880 confocal microscope coupled with an Airyscan module. Processing of the raw Airyscan images was performed on the ZEN Black software.

Immunoblot analysis. Cell pellets were lysed in sample buffer (200 mM Tris-HCl, pH 6.8, 5.2% SDS, 20% glycerol, 0.1% bromophenol blue, 5% β-mercaptoethanol), resolved by SDS–PAGE and analysed by immunoblotting using primary antibodies specific for human DDX42 (HPA023571, Sigma-Aldrich), Flag (M2, Sigma-Aldrich) and Actin (A1978, Sigma-Aldrich), followed by secondary horseradish peroxidase-conjugated anti-mouse or anti-rabbit immunoglobulin antibodies and chemiluminescence (Bio-Rad). Images were acquired on a ChemiDoc™ gel imaging system (Bio-Rad).

IAV production and infection

We have described previously IAV NanoLuciferase reporter virus generation (Doyle et al., 2018). Stocks were titrated by plaque assays on MDCK cells. IAV challenges were performed in serum-free DMEM for 1 h and the medium was subsequently replaced with DMEM containing 10%. IAV infection experiments were performed in triplicates in 96-well plates with cultures maintained for 16 h post-challenge. NanoLuciferase activity was measured with the Nano-Glo assay system (Promega), and luminescence was detected using a plate reader (Infinite® 200 PRO, Tecan).

VSV production and infection. A VSV-G pseudotyped-VSV-Δenv reporter virus, coding both GFP and Firefly Luciferase, was obtained from Gert Zimmer (Rentsch and Zimmer, 2011). The virus was amplified on pMD.G transfected 293T and titrated thanks to the GFP reporter gene. For infection, 2.5 x 10^4 cells per well in 96-well plates were infected at the indicated MOIs. 24h after infection, cells were lysed and Firefly luciferase activity was measured (Firefly luciferase Assay System Promega).

ZIKV production and infection. The nanoluciferase expressing ZIKV construct has been described (Mutso et al., 2017). The corresponding linearized plasmid was transcribed in vitro using the SP6 mMESSAGE mMACHINE™ (Thermofischer Scientific) and HEK293T cells were transfected with the transcribed RNA. After 7 days, supernatants were harvested, filtered and stock titers were determined by plaque assays on Vero cells. For infections, 2.5 x 10^4 cells per well in 96-well plates were infected, at the indicated MOIs. 24h after infection, cells were lysed and Nanoluciferase activity was measured using the Kit Nano Glo luciferase Assay (Promega).

CHIKV production and infection. The Nanoluciferase luciferase coding CHIKV construct was a gift from Andres Merits. The linearized plasmid coding CHIKV genome was transcribed with the T7 mMESSAGE mMACHINE kit (Thermofischer Scientific) and 5 x 10^5 HEK293T were transfected with 1-4 μg of transcribed RNA, using Lipofectamine 2000 (Thermofischer Scientific). After 24h, supernatants were harvested, filtered and viruses were then amplified on baby hamster kidney (BHK21) cells. Stock titers were determined by plaque assays on Vero cells. For infections, 2.5 x 10^4 cells per well in 96-well plates were infected at the indicated MOIs. 24h after infection, cells were lysed and Nanoluciferase activity was measured.

SARS-CoV-2 production and infection

The SARS-CoV-2 BetaCoV/France/IDF0372/2020 isolate was supplied by Pr. Sylvie van der Werf and the National Reference Centre for Respiratory Viruses hosted by Institut Pasteur (Paris, France). The virus was amplified in Vero E6 cells (MOI 0,005) in serum-free media supplemented with 0,1 μg/ml L-1-p-Tosylamino-2-phenylethyl chloromethylketone (TPCK)-treated trypsin (Sigma-Aldrich). The supernatant was harvested at 72 h post infection when cytopathic effects were observed (with around 50% cell death), cell debris were removed by centrifugation, and aliquots stored at -80C. Viral supernatants were titrated by plaque assays in Vero E6 cells. Typical titers were 5.10^6 plaque forming units (PFU)/ml.

Infections of A549-ACE2 cells were performed at the indicated multiplicity of infection (MOI; as

calculated from titers obtained in Vero E6 cells) in serum-free DMEM and 5% serum-containing DMEM, respectively. The viral input was left for the duration of the experiment and cells lysed at 48 h post-infection for RT-qPCR analysis.

Data availability

The datasets generated during and/or analysed during the current study are available from the corresponding authors on reasonable request.

Requests for materials

Requests for material should be addressed to Caroline Goujon at the corresponding address above.

Acknowledgements

We wish to thank Tom Doyle and Chad Swanson for their useful comments on the manuscript, and Matthieu Lewis, Nadine Laguette, Emiliano Ricci, Nathalie Arhel, Juliette Fernandez, Jean-Luc Battini, Georg Kochs, Andres Merits and Nathan Sherer for the generous provision of reagents, protocols and/or for helpful discussions. We are grateful to Nicolas Manel and Helena Izquierdo-Fernandez for sharing their protocol for efficient knockdown in primary CD4+ T cell using CRISPR/Cas9 RNP electroporation. We are grateful to Myriam Boyer, Stéphanie Viala, Baptiste Monterroso and Orestis Faklaris from the imaging and flow cytometry facility MRI, for advice with flow cytometry and confocal microscopy, respectively. This work was supported by the Institut National de la Santé et de la Recherche Médicale (INSERM) (to CG), the ATIP-Avenir programme (to CG), institutional funds from the Centre National de la Recherche Scientifique (CNRS) and Montpellier University, France REcherche Nord&Sud Sida/HIV et Hépatites (ANRS) (ECTZ21792 to CG; ECTZ35478 to OM), Sidaction (to CG), a Starting Grant from the European Research Council (759226, ANTIViR) (to CG), PhD studentships from the Ministry of Higher Education and Research (to BB, JM and AR), and a 4th year PhD studentship from the Fondation pour la Recherche Médicale (to BB). SR and HP acknowledge financial support from the France Génomique National infrastructure, funded as part of “Investissement d’Avenir” program managed by Agence Nationale de la Recherche (contract ANR-10-INBS-09). We acknowledge the imaging facility MRI, member of the national infrastructure France-BioImaging supported by

the French National Research Agency (ANR-10-INBS-04) and the BSL-3 facility CEMIPAI (UMS 3725 CNRS Montpellier University).

Author contributions

B.B. and CG designed the study, analysed the data and wrote the manuscript. B.B. and C.G. performed the whole-genome screens and candidate validation. B.B. carried out most of the experiments, with technical assistance from A.R., F.G.d.G, J.M., M.T., W.D., A.M., and O.M.; V.C. provided some of the lentiviral vector stocks; E.B. and L.B. performed CHIKV infections and N.G. ZIKV infections; H.P. and S.R. performed the Illumina sequencing and MaGECK analyses, respectively. All authors have read and approved the manuscript.

Conflicts of interest statement

The authors have no conflicts of interest to declare in relation to this manuscript.

References

Adachi, A., Gendelman, H.E., Koenig, S., Folks, T., Willey, R., Rabson, A., and Martin, M.A. (1986). Production of acquired immunodeficiency syndrome-associated retrovirus in human and nonhuman cells transfected with an infectious molecular clone. J. Virol. *59*, 284–291.

Bainbridge, J.W., Stephens, C., Parsley, K., Demaison, C., Halfyard, A., Thrasher, A.J., and Ali, R.R. (2001). In vivo gene transfer to the mouse eye using an HIV-based lentiviral vector; efficient long-term transduction of corneal endothelium and retinal pigment epithelium. Gene Ther. *8*, 1665–1668.

Bulli, L., Apolonia, L., Kutzner, J., Pollpeter, D., Goujon, C., Herold, N., Schwarz, S.-M., Giernat, Y., Keppler, O.T., Malim, M.H., et al. (2016). Complex interplay between HIV-1 Capsid and MX2-independent IFNα-induced antiviral factors. J. Virol.

Burdick, R.C., Li, C., Munshi, M., Rawson, J.M.O., Nagashima, K., Hu, W.-S., and Pathak, V.K. (2020). HIV-1 uncoats in the nucleus near sites of integration. Proc. Natl. Acad. Sci. *117*, 5486–5493.

Chemudupati, M., Kenney, A.D., Bonifati, S., Zani, A., McMichael, T.M., Wu, L., and Yount, J.S. (2019). From APOBEC to ZAP: Diverse mechanisms used by cellular restriction factors to inhibit virus infections. Biochim. Biophys. Acta Mol. Cell Res. *1866*, 382–394.

Corman, V.M., Landt, O., Kaiser, M., Molenkamp, R., Meijer, A., Chu, D.K., Bleicker, T., Brünink, S., Schneider, J., Schmidt, M.L., et al. (2020). Detection of 2019 novel coronavirus (2019-nCoV) by real-time RT-PCR. Euro Surveill. Bull. Eur. Sur Mal. Transm. Eur. Commun. Dis. Bull. *25*.

Dharan, A., Bachmann, N., Talley, S., Zwikelmaier, V., and Campbell, E.M. (2020). Nuclear pore blockade reveals that HIV-1 completes reverse transcription and uncoating in the nucleus. Nat. Microbiol.

Doench, J.G. (2018). Am I ready for CRISPR? A user's guide to genetic screens. Nat. Rev. Genet. *19*, 67–80.

Doyle, T., Goujon, C., and Malim, M.H. (2015). HIV-1 and interferons: who's interfering with whom? Nat. Rev. Microbiol. *13*, 403–413.

Doyle, T., Moncorgé, O., Bonaventure, B., Pollpeter, D., Lussignol, M., Tauziet, M., Apolonia, L., Catanese, M.-T., Goujon, C., and Malim, M.H. (2018). The interferon-inducible isoform of NCOA7 inhibits endosome-mediated viral entry. Nat. Microbiol. *3*, 1369–1376.

Faulkner, G.J., and Billon, V. (2018). L1 retrotransposition in the soma: a field jumping ahead. Mob. DNA *9*, 22.

Fay, M.M., Lyons, S.M., and Ivanov, P. (2017). RNA G-Quadruplexes in Biology: Principles and Molecular Mechanisms. J. Mol. Biol. *429*, 2127–2147.

Gaddis, N.C., Sheehy, A.M., Ahmad, K.M., Swanson, C.M., Bishop, K.N., Beer, B.E., Marx, P.A., Gao, F., Bibollet-Ruche, F., Hahn, B.H., et al. (2004). Further Investigation of Simian Immunodeficiency Virus Vif Function in Human Cells. J. Virol. *78*, 12041–12046.

Ghimire, D., Rai, M., and Gaur, R. (2018). Novel host restriction factors implicated in HIV-1 replication. J. Gen. Virol. *99*, 435–446.

Goodier, J.L., Cheung, L.E., and Kazazian, H.H. (2012). MOV10 RNA Helicase Is a Potent Inhibitor of Retrotransposition in Cells. PLoS Genet. *8*, e1002941.

Goujon, C., and Malim, M.H. (2010). Characterization of the alpha interferon-induced postentry block to HIV-1 infection in primary human macrophages and T cells. J. Virol. *84*, 9254–9266.

Goujon, C., Arfi, V., Pertel, T., Luban, J., Lienard, J., Rigal, D., Darlix, J.-L., and Cimarelli, A. (2008). Characterization of Simian Immunodeficiency Virus SIVSM/Human Immunodeficiency Virus Type 2 Vpx Function in Human Myeloid Cells. J. Virol. *82*, 12335–12345.

Goujon, C., Moncorgé, O., Bauby, H., Doyle, T., Ward, C.C., Schaller, T., Hué, S., Barclay, W.S., Schulz, R., and Malim, M.H. (2013a). Human MX2 is an interferon-induced post-entry inhibitor of HIV-1 infection. Nature *502*, 559–562.

Goujon, C., Schaller, T., Galão, R.P., Amie, S.M., Kim, B., Olivieri, K., Neil, S.J.D., and Malim, M.H. (2013b). Evidence for IFNα-induced, SAMHD1-independent inhibitors of early HIV-1 infection. Retrovirology *10*, 23.

Granneman, S., Bernstein, K.A., Bleichert, F., and Baserga, S.J. (2006). Comprehensive Mutational Analysis of Yeast DEXD/H Box RNA Helicases Required for Small Ribosomal Subunit Synthesis. Mol. Cell. Biol. *26*, 1183–1194.

Haller, O., Staeheli, P., Schwemmle, M., and Kochs, G. (2015). Mx GTPases: dynamin-like antiviral machines of innate immunity. Trends Microbiol. *23*, 154–163.

Jimenez-Guardeño, J.M., Apolonia, L., Betancor, G., and Malim, M.H. (2019). Immunoproteasome activation enables human TRIM5α restriction of HIV-1. Nat. Microbiol.

Kane, M., Yadav, S.S., Bitzegeio, J., Kutluay, S.B., Zang, T., Wilson, S.J., Schoggins, J.W., Rice, C.M., Yamashita, M., Hatziioannou, T., et al. (2013). MX2 is an interferon-induced inhibitor of HIV-1 infection. Nature *502*, 563–566.

Langmead, B., Trapnell, C., Pop, M., and Salzberg, S.L. (2009). Ultrafast and memory-efficient alignment of short DNA sequences to the human genome. Genome Biol. *10*, R25.

Li, H., Handsaker, B., Wysoker, A., Fennell, T., Ruan, J., Homer, N., Marth, G., Abecasis, G., Durbin, R., and 1000 Genome Project Data Processing Subgroup (2009). The Sequence Alignment/Map format and SAMtools. Bioinforma. Oxf. Engl. *25*, 2078–2079.

Li, W., Xu, H., Xiao, T., Cong, L., Love, M.I., Zhang, F., Irizarry, R.A., Liu, J.S., Brown, M., and Liu, X.S. (2014). MAGeCK enables robust identification of essential genes from genome-scale CRISPR/Cas9 knockout screens. Genome Biol. *15*, 554.

Liu, N., Lee, C.H., Swigut, T., Grow, E., Gu, B., Bassik, M.C., and Wysocka, J. (2018). Selective silencing of euchromatic L1s revealed by genome-wide screens for L1 regulators. Nature *553*, 228–232.

Liu, Z., Pan, Q., Liang, Z., Qiao, W., Cen, S., and Liang, C. (2015). The highly polymorphic cyclophilin A-binding loop in HIV-1 capsid modulates viral resistance to MxB. Retrovirology *12*, 1.

Martin, M. (2011). Cutadapt removes adapter sequences from high-throughput sequencing reads. EMBnet.Journal *17*, 10–12.

Moncorge, O., Long, J.S., Cauldwell, A.V., Zhou, H., Lycett, S.J., and Barclay, W.S. (2013). Investigation of Influenza Virus Polymerase Activity in Pig Cells. J. Virol. *87*, 384–394.

Moran, J.V., Holmes, S.E., Naas, T.P., DeBerardinis, R.J., Boeke, J.D., and Kazazian, H.H. (1996). High frequency retrotransposition in cultured mammalian cells. Cell *87*, 917–927.

Mutso, M., Saul, S., Rausalu, K., Susova, O., Žusinaite, E., Mahalingam, S., and Merits, A. (2017). Reverse genetic system, genetically stable reporter viruses and packaged subgenomic replicon based on a Brazilian Zika virus isolate. J. Gen. Virol. *98*, 2712–2724.

Naldini, L., Blömer, U., Gallay, P., Ory, D., Mulligan, R., Gage, F.H., Verma, I.M., and Trono, D. (1996). In vivo gene delivery and stable transduction of nondividing cells by a lentiviral vector. Science *272*, 263–267.

Ochsenbauer, C., Edmonds, T.G., Ding, H., Keele, B.F., Decker, J., Salazar, M.G., Salazar-Gonzalez, J.F., Shattock, R., Haynes, B.F., Shaw, G.M., et al. (2012). Generation of transmitted/founder HIV-1 infectious molecular clones and characterization of their replication capacity in CD4 T lymphocytes and monocyte-derived macrophages. J. Virol. *86*, 2715–2728.

OhAinle, M., Helms, L., Vermeire, J., Roesch, F., Humes, D., Basom, R., Delrow, J.J., Overbaugh, J., and Emerman, M. (2018). A virus-packageable CRISPR screen identifies host factors

mediating interferon inhibition of HIV. ELife *7*.

O'Rourke, J.P., Newbound, G.C., Kohn, D.B., Olsen, J.C., and Bunnell, B.A. (2002). Comparison of gene transfer efficiencies and gene expression levels achieved with equine infectious anemia virus- and human immunodeficiency virus type 1-derived lentivirus vectors. J. Virol. *76*, 1510–1515.

Ostertag, E.M., Prak, E.T., DeBerardinis, R.J., Moran, J.V., and Kazazian, H.H. (2000). Determination of L1 retrotransposition kinetics in cultured cells. Nucleic Acids Res. *28*, 1418–1423.

Peng, K., Muranyi, W., Glass, B., Laketa, V., Yant, S.R., Tsai, L., Cihlar, T., Müller, B., and Kräusslich, H.-G. (2014). Quantitative microscopy of functional HIV post-entry complexes reveals association of replication with the viral capsid. ELife *3*, e04114.

Pohjala, L., Utt, A., Varjak, M., Lulla, A., Merits, A., Ahola, T., and Tammela, P. (2011). Inhibitors of Alphavirus Entry and Replication Identified with a Stable Chikungunya Replicon Cell Line and Virus-Based Assays. PLOS ONE *6*, e28923.

Rentsch, M.B., and Zimmer, G. (2011). A Vesicular Stomatitis Virus Replicon-Based Bioassay for the Rapid and Sensitive Determination of Multi-Species Type I Interferon. PLoS ONE *6*.

Rocak, S. (2005). Characterization of the ATPase and unwinding activities of the yeast DEAD-box protein Has1p and the analysis of the roles of the conserved motifs. Nucleic Acids Res. *33*, 999–1009.

Ruggiero, E., and Richter, S.N. (2018). G-quadruplexes and G-quadruplex ligands: targets and tools in antiviral therapy. Nucleic Acids Res. *46*, 3270–3283.

Ryan-Graham, M.A., and Peden, K.W.C. (1995). Both Virus and Host Components Are Important for the Manifestation of a Nef- Phenotype in HIV-1 and HIV-2. Virology *213*, 158–168.

Saenz, D.T., Teo, W., Olsen, J.C., and Poeschla, E.M. (2005). Restriction of feline immunodeficiency virus by Ref1, Lv1, and primate TRIM5alpha proteins. J. Virol. *79*, 15175–15188.

Sanjana, N.E., Shalem, O., and Zhang, F. (2014). Improved vectors and genome-wide libraries for CRISPR screening. Nat. Methods *11*, 783–784.

Schaller, T., Ocwieja, K.E., Rasaiyaah, J., Price, A.J., Brady, T.L., Roth, S.L., Hué, S., Fletcher, A.J., Lee, K., KewalRamani, V.N., et al. (2011). HIV-1 capsid-cyclophilin interactions determine nuclear import pathway, integration targeting and replication efficiency. PLoS Pathog. *7*, e1002439.

Schindelin, J., Arganda-Carreras, I., Frise, E., Kaynig, V., Longair, M., Pietzsch, T., Preibisch, S., Rueden, C., Saalfeld, S., Schmid, B., et al. (2012). Fiji: an open-source platform for biological-image analysis. Nat. Methods *9*, 676–682.

Shalem, O., Sanjana, N.E., Hartenian, E., Shi, X., Scott, D.A., Mikkelsen, T.S., Heckl, D., Ebert, B.L., Root, D.E., Doench, J.G., et al. (2014). Genome-scale CRISPR-Cas9 knockout screening in human cells. Science *343*, 84–87.

Shalem, O., Sanjana, N.E., and Zhang, F. (2015). High-throughput functional genomics using CRISPR-Cas9. Nat. Rev. Genet. *16*, 299–311.

Simon, J.H., Southerling, T.E., Peterson, J.C., Meyer, B.E., and Malim, M.H. (1995). Complementation of vif-defective human immunodeficiency virus type 1 by primate, but not nonprimate, lentivirus vif genes. J. Virol. *69*, 4166–4172.

Taschuk, F., and Cherry, S. (2020). DEAD-Box Helicases: Sensors, Regulators, and Effectors for Antiviral Defense. Viruses *12*.

Uhlmann-Schiffler, H., Jalal, C., and Stahl, H. (2006). Ddx42p--a human DEAD box protein with RNA chaperone activities. Nucleic Acids Res. *34*, 10–22.

Uhlmann-Schiffler, H., Kiermayer, S., and Stahl, H. (2009). The DEAD box protein Ddx42p modulates the function of ASPP2, a stimulator of apoptosis. Oncogene *28*, 2065–2073.

Wei, J., Alfajaro, M.M., DeWeirdt, P.C., Hanna, R.E., Lu-Culligan, W.J., Cai, W.L., Strine, M.S., Zhang, S.-M., Graziano, V.R., Schmitz, C.O., et al. (2020). Genome-wide CRISPR screens reveal host factors critical for SARS-CoV-2 infection. Cell.

Will, C.L., Urlaub, H., Achsel, T., Gentzel, M., Wilm, M., and Lührmann, R. (2002). Characterization of novel SF3b and 17S U2 snRNP proteins, including a human Prp5p homologue and an SF3b DEAD-box protein. EMBO J. *21*, 4978–4988.

Wingett, S.W., and Andrews, S. (2018). FastQ Screen: A tool for multi-genome mapping and quality control. F1000Research *7*, 1338.

Xu, B., Pan, Q., and Liang, C. (2018). Role of MxB in Alpha Interferon-Mediated Inhibition of HIV-1 Infection. J. Virol. *92*.

Zyner, K.G., Mulhearn, D.S., Adhikari, S., Martínez Cuesta, S., Di Antonio, M., Erard, N., Hannon, G.J., Tannahill, D., and Balasubramanian, S. (2019). Genetic interactions of G-quadruplexes in humans. ELife *8*, e46793.

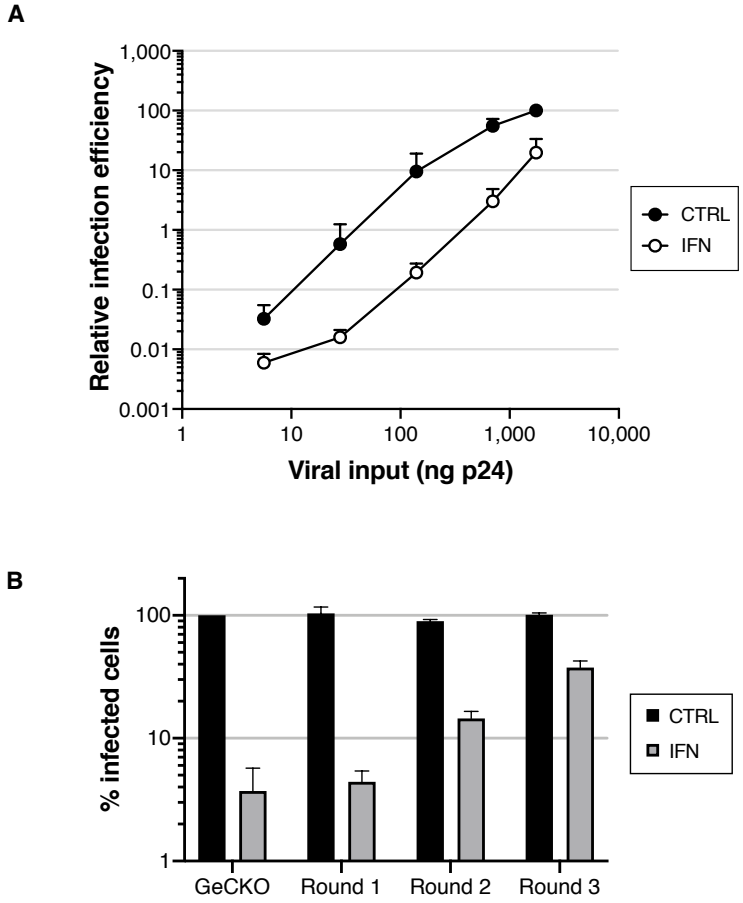

Figure S1. Related to Figure 1.

A. IFN pre-treatment potently inhibits HIV-1 infection in T98G cells and is, at least partially, saturable. T98G/Cas9/CD4/CXCR4/ Firefly cells were pre-treated with IFN for 24 h prior to infection with increasing doses of NL4-3 Renilla (indicated in ng $p24^{Gag}$). Renilla activity was normalized to Firefly activity and the relative infection efficiencies are shown. Data represent the average of 3 independent experiments and one standard deviation from the mean.

B. GeCKO screen validation. GeCKO control cells and enriched cells from 3 successive rounds of selection (Round 1, 2, and 3, as indicated) were treated with IFN or not and infected with GFP-expressing lentiviral vectors. The percentage of infected cells was evaluated by flow cytometry 2 days post-infection. Data represent the average of 2 independent experiments and one standard deviation from the mean.

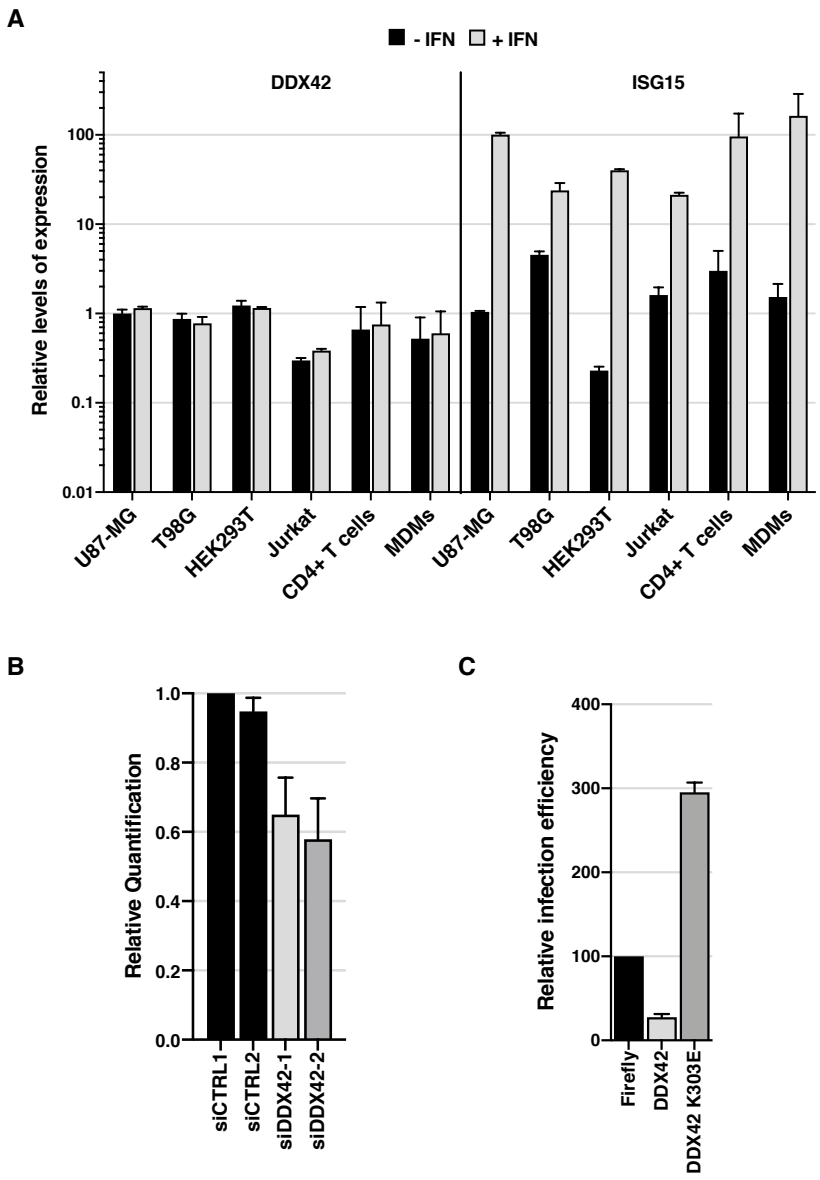

Figure S2. Related to Figure 2.

A. DDX42 is not an ISG. The indicated primary cells or immortalized cell cultures were treated with IFN for 24 h or left untreated. RNA was subsequently extracted and DDX42 and ISG15 (a prototype ISG) mRNA levels were quantified by RT-qPCR; Actin B and GAPDH were used as endogenous controls. The bar chart shows the relative levels of expression of DDX42 and ISG15 in the presence or absence of IFN treatment. Data represent the mean ± S.E.M of three independent experiments.

B. DDX42 silencing efficiency in monocyte-derived macrophages. siRNA-transfected MDMs were harvested 48h post-transfection for RNA extraction and quantification of DDX42 mRNA levels by RT-qPCR. Actin and GAPDH were used as endogenous controls. Data represent the mean ± S.E.M of three independent experiments performed with cells from 3 different blood donors (parallel samples from Figure 2E).

C. Ectopic expression of DDX42 K303E mutant increases HIV-1 infection. U87-MG/CD4/CXCR4 cells were transduced with lentiviral vectors expressing either Firefly (negative control), WT DDX42 (DDX42) or a motif I mutant DDX42 K303, which has an impaired ATPase activity (DDX42 K303E). Transduced cells were infected with NL4-3 Renilla and the infection efficiency was assessed 24h later by measuring Renilla activity. Data represent the mean ± S.E.M of four independent experiments.

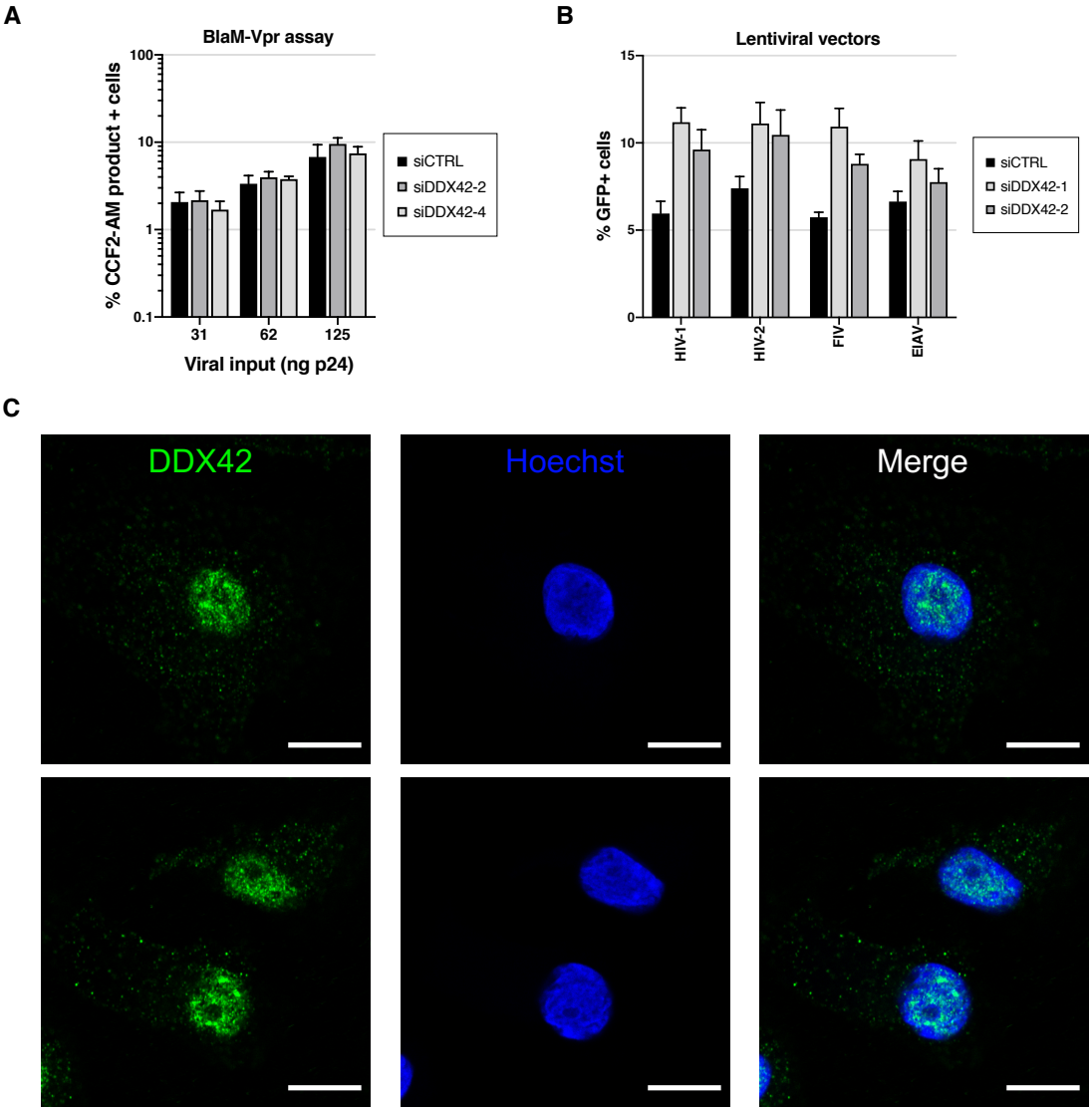

Figure S3. Related to Figure 3.

A. DDX42 depletion does not affect HIV-1 entry. DDX42-depleted U87-MG/CD4/CXCR4 cells were infected with the indicated amounts of viruses carrying the β-lactamase (BlaM)-Vpr fusion protein for 3 hours. The cells were subsequently loaded with CCF2-AM substrate dye for 2h, washed extensively and incubated for another 16h for the reaction to develop. Cells positive for the CCF2-AM product were scored by flow cytometry. Data represent the mean ± S.E.M of three independent experiments.

B. Effect of DDX42 on lentiviral vectors. U87-MG/CD4/CXCR4 cells were transfected with non-targeting siRNA (siCTRL) or siRNAs targeting DDX42 (siDDX42-1, -2, and -4) and, 72 h later, the cells infected with HIV-1- HIV-2- FIV- EIAV-based, GFP-coding LVs at a MOI of 0,1. Infection efficiency was scored 24 h by measuring the percentage of GFP expressing cells by flow cytometry. Data represent the mean ± S.E.M of three independent experiments.

C. DDX42 localization in MDMs. MDMs were fixed, endogenous DDX42 and the nuclei were visualized using DDX42-specific antibodies and Hoechst staining, respectively, and confocal microscopy. Representative images are shown. Scale bar, 10 μm.

Supplemental methods

Only the methods specific for the supplemental figures are presented here.

Plasmids.

pBlaM-Vpr and pAdVAntage have been described (Cavrois et al., 2002).

Lentiviral production.

β-lactamase-Vpr (BlaM-Vpr)-carrying viruses, bearing the wild-type Env, were produced by co-transfection of HEK293T cells with the NL4-3/Nef-IRES-Renilla provirus expression vector, pBlaM-Vpr and pAdVAntage at a ratio of 4:1:0.5, as previously described (Cavrois et al., 2002). Viral particles were titrated using an HIV-1 $p24^{Gag}$ Alpha-Lisa kit and an Envision plate reader (Perkin Elmer).

Quantification of mRNA expression.

TaqMan gene expression assays (Applied Biosystem) specific for ISG15: Hs00192713_m1.

BlaM-Vpr assay for HIV-1 entry. These assays were performed as described previously (Goujon and Malim, 2010). Briefly, 2 x 10^5 U87-MG/CD4/CXCR4 cells were plated in 24-well plates and incubated with BlaM-Vpr carrying NL4-3 particles (31, 62, 125 ng $p24^{Gag}$) or mock-infected for 3 h at 37°C. The cells were then washed once in CO_2-independent medium and loaded with CCF2-AM substrate-containing solution (ThermoFisher Scientific) for 1 h at room temperature before 2 washes and incubation at room temperature for 16 h in development medium (CO_2-independent medium containing 2,5 mM probenecid). Finally, the cells were trypsinized, washed and fixed in 1% paraformaldehyde (PFA)-PBS1X before analysis with a FACSCanto™ II (Becton Dickinson).

Supplementary Information References

Cavrois, M., de Noronha, C., and Greene, W.C. (2002). A sensitive and specific enzyme-based assay detecting HIV-1 virion fusion in primary T lymphocytes. Nat Biotechnol *20*, 1151–1154.

Goujon, C., and Malim, M.H. (2010). Characterization of the alpha interferon-induced postentry block to HIV-1 infection in primary human macrophages and T cells. J. Virol. *84*, 9254–9266.